

1 **Infection of human lymphomononuclear cells by SARS-CoV-2**

2

3 Marjorie C Pontelli**¹, Italo A Castro**¹, Ronaldo B Martins¹, Flávio P Veras²,
4 Leonardo La Serra¹, Daniele C Nascimento², Ricardo S Cardoso¹, Roberta
5 Rosales⁶, Thais M Lima¹, Juliano P Souza¹, Diego B Caetité², Mikhael H F de
6 Lima², Juliana T Kawahisa², Marcela C Giannini^{2,3}, Letícia P Bonjorno^{2,3}, Maria I
7 F Lopes^{2,3}, Sabrina S Batah⁸, Li Siyuan⁸, Rodrigo L Assad^{2,3}, Sergio C L
8 Almeida^{2,3}, Fabiola R Oliveira^{2,3}, Maíra N Benatti^{2,3}, Lorena L F Pontes⁷,
9 Rodrigo C Santana^{2,4}, Fernando C Vilar^{2,4}, Maria A Martins^{2,5}, Thiago M
10 Cunha², Rodrigo T Calado⁷, José C Alves-Filho², Dario S Zamboni^{2,6}, Alexandre
11 Fabro⁸, Paulo Louzada-Junior^{2,3}, Rene D R Oliveira^{2,3}, Fernando Q Cunha²,
12 Eurico Arruda*¹.

13

14 1 Virology Research Center, Ribeirao Preto Medical School; 2 Center of
15 Research in Inflammatory Diseases (CRID), 3 Divisions of Clinical Immunology;
16 4 Infectious Diseases, 5 Intensive Care Unit; 6 Department of Cell and
17 Molecular Biology and Pathogenic Bioagents, Ribeirao Preto Medical School; 7
18 Blood Center of Ribeirao Preto, Ribeirao Preto, Brazil; 8 Department of
19 Pathology, Ribeirao Preto Medical School,
20 University of Sao Paulo, Ribeirao Preto, Sao Paulo, Brazil

21

22 +Contributed equally to the study

23 *Corresponding authors:

24

25 Marjorie Cornejo Pontelli; Virology Research Center, Ribeirao Preto Medical
26 School, 3900 Bandeirantes Av, 14049-900, Ribeirao Preto –SP – Brazil. Tel.:
27 +55 16 33154508, Email: marpontelli@gmail.com

28

29 Italo Araujo Castro; Virology Research Center, Ribeirao Preto Medical School,
30 3900 Bandeirantes Av, 14049-900, Ribeirao Preto –SP – Brazil. Tel.: +55 16
31 33154508, Email: italo.a.castro@gmail.com

32

33 Eurico Arruda; Virology Research Center, Ribeirao Preto Medical School, 3900
34 Bandeirantes Av, 14049-900, Ribeirao Preto –SP – Brazil. Tel.: +55 16
35 33153337, Email: eaneto@fmrp.usp.br

36

37 **Abstract.** Although SARS-CoV-2 severe infection is associated with a
38 hyperinflammatory state, lymphopenia is an immunological hallmark, and
39 correlates with poor prognosis in COVID-19. However, it remains unknown if
40 circulating human lymphocytes and monocytes are susceptible to SARS-CoV-2
41 infection. In this study, SARS-CoV-2 infection of human peripheral blood
42 mononuclear cells (PBMCs) was investigated both *in vitro* and *in vivo*. We found
43 that *in vitro* infection of whole PBMCs from healthy donors was productive of
44 virus progeny. Results revealed that monocytes, as well as B and T
45 lymphocytes, are susceptible to SARS-CoV-2 active infection and viral
46 replication was indicated by detection of double-stranded RNA. Moreover, flow
47 cytometry and immunofluorescence analysis revealed that SARS-CoV-2 was
48 frequently detected in monocytes and B lymphocytes from COVID-19 patients,
49 and less frequently in CD4⁺T lymphocytes. The rates of SARS-CoV-2-infected
50 monocytes in PBMCs from COVID-19 patients increased over time from
51 symptom onset. Additionally, SARS-CoV-2-positive monocytes and B and
52 CD4⁺T lymphocytes were detected by immunohistochemistry in post mortem
53 lung tissue. SARS-CoV-2 infection of blood circulating leukocytes in COVID-19
54 patients may have important implications for disease pathogenesis, immune
55 dysfunction, and virus spread within the host.

56

57

58

Introduction

59

60 In December 2019, a new coronavirus emerged as the cause of a severe
61 acute respiratory disease named Coronavirus-related disease 2019 (COVID-
62 19). The virus that spilled over to humans in China was classified in the family
63 *Coronaviridae*, genus *Betacoronavirus*, and was named Severe Acute
64 Respiratory Syndrome Coronavirus 2 (SARS-CoV-2), for its similarity to SARS-
65 CoV [1].

66 Since its emergence, SARS-CoV-2 has spread to 185 countries/political
67 regions and infected more than 11 million people worldwide, with a death toll of
68 approximately 500,000 cases. The main clinical features of COVID-19 are fever,
69 dry cough, dyspnea and myalgia, but some patients rapidly evolve to severe
70 respiratory distress syndrome [2].

71 Previous studies have shown that inflammatory cytokine storm and
72 lymphocytopenia are important markers of severe COVID-19 cases, with severe
73 functional exhaustion of TCD4+ and TCD8+ lymphocytes [2–4]. Interestingly,
74 peripheral blood mononuclear cells (PBMCs) from COVID-19 patients showed
75 upregulation of autophagy and apoptosis pathways [5], suggesting that
76 dampening of the immune system by SARS-CoV-2 infection may have a strong
77 impact on the clinical outcome of severe COVID-19.

78 A decrease in circulating lymphocytes has been associated with poor
79 COVID-19 outcome, but it is still unclear whether that lymphopenia is directly
80 due to SARS-CoV-2 infection of lymphocytes with consequent cell death.
81 SARS-CoV-2 interacts with target cells via binding of its major surface
82 glycoprotein spike (S) with the angiotensin-converting enzyme 2 (ACE2)
83 present in the cell membrane [6]. ACE2-independent cell-entry has also been
84 reported and could be an alternative mechanism of SARS-CoV-2 entry in cells
85 with low ACE2 expression [7]. Cleavage of the S protein is required for efficient
86 entry of SARS-CoV-2, which is accomplished by transmembrane serine
87 protease TMPRSS2 [6].

88 In addition to respiratory disease, COVID-19 patients frequently develop
89 gastrointestinal symptoms, which is in keeping with the high expression of
90 TMPRSS2 and ACE2 documented in enterocytes [8]. Furthermore, the SARS-

91 CoV-2 antigen was found *post mortem* in the spleen and lymph nodes with
92 pathological signs of damage. In these organs, monocytes do contain viral
93 antigens, but it was not clear whether this was due to active viral replication or
94 phagocytosis, nor if monocytes become infected before reaching secondary
95 lymphoid tissues [9]. While SARS-CoV-2 causes viremia, until now, infectious
96 SARS-CoV-2 was not successfully isolated from peripheral blood in COVID-19
97 patients, and it is suggested that the virus in blood may be cell-associated [5, 9].
98 In this study, we investigated the susceptibility and permissiveness of human
99 peripheral blood mononuclear cells (PBMC) to SARS-CoV-2. We found that
100 PBMCs are susceptible and permissive to SARS-CoV-2 infection, both *in vivo*
101 and *ex vivo*, which seems to play a direct role in the reduction of circulating
102 lymphocytes.

103

104 **Patients and Methods**

105

106 **Ethical statement and COVID-19 patients.** The study was approved by the
107 National Ethics Committee (CONEP, CAAE: 30248420.9.0000.5440 and
108 31797820.8.0000.5440). A total of 29 hospitalized patients were enrolled, all
109 with clinical and radiological features of COVID-19 and confirmed SARS-CoV-2
110 infection by RT-PCR in respiratory secretions, with detection of specific IgM or
111 IgG antibodies to SARS-CoV-2. Clinical features, laboratory results and drug
112 therapies are summarized in **Supplementary Table 1**. For all comparisons, 12
113 age and gender-matching healthy controls were also enrolled. Written informed
114 consent was obtained for both patients and healthy controls.

115

116 **Production of mouse anti-SARS-CoV-2 hyperimmune serum.** Male C57Bl/6
117 mice were bred and maintained under specific pathogen-free conditions at the
118 animal facility of the Ribeirão Preto Medical School (FMRP) at University of São
119 Paulo. The protocol for production of mouse hyperimmune serum were carried
120 out with 8-week-old male mice following the institutional guidelines on ethics in
121 animal experiments and was approved by the University of São Paulo Ethics
122 Committee for Animal Experimental Research - CETEA (Protocol no. 001/2020-
123 1). To immunize animals, virus stock was inactivated by adding formaldehyde to

124 a final concentration of 0.2%, and incubated overnight at 37°C. Then, virus was
125 purified by ultracentrifugation (10% sucrose cushion, 159.000 × g for 1h). The
126 pellet was resuspended with Phosphate Buffer Saline (PBS) 1x and stored at -
127 20°C. In order to confirm inactivation, titration of the inactivated product was
128 done both by TCID₅₀ and by plaque assay in Vero-E6 cells with 5-day
129 incubation, without any cytopathic effects. Three C57Bl/6 mice were inoculated
130 intramuscularly with an emulsion containing the equivalent of 10⁶ TCID₅₀ of
131 inactivated SARS-CoV-2 in complete Freund's adjuvant (CFA, BD, cat. 263810)
132 diluted 1:1 in PBS. Boosts were given with inactivated SARS-CoV-2 in
133 incomplete Freund's adjuvant (without *M. tuberculosis*, IFA, BD, cat. 263910) on
134 days 7 and 14 after the first immunization. One week after the last dose,
135 animals were euthanized with an excess of anesthetics xylazine (60 mg/kg) and
136 ketamine (300 mg/kg), following exsanguination by cardiac puncture. Animal
137 serum conversion was evaluated by indirect immunofluorescence using slide
138 preparations of SARS-CoV-2 infected Caco-2 cells, fixed with 4%
139 paraformaldehyde and AlexaFluor 488-labelled rabbit anti-mouse secondary
140 antibody. Coverslips were analyzed using an optic microscope (Olympus
141 BX40).

142

143 **Isolation of peripheral blood mononuclear cells (PBMCs).** Human PBMCs
144 were isolated from COVID-19 patients or healthy donors by density gradient
145 using Percoll (GE Healthcare, cat. 17-5445-01), as previously described [10,
146 11]. PBMCs were washed, resuspended in RPMI 1640 supplemented with 10%
147 fetal bovine serum (FBS) and kept on ice until further use.

148

149 **Virus and cell lines.** The passage 1 (P1) of SARS-CoV-2 Brazil/SPBR-02/2020
150 isolate obtained in Vero-E6 from a COVID-19 patient in Sao Paulo was kindly
151 provided by Prof. Edison Durigon (ICB-USP). P1 was diluted 1:1000 in
152 Dulbecco's modified Eagle's medium (DMEM) and inoculated in Vero-E6 cells
153 monolayers to produce the P2 stock. For stock titration, serial 10-fold dilutions
154 were inoculated in quadruplicate monolayers of Vero-E6 cells and incubated at
155 37°C in 5% CO₂. On the fourth day of incubation, the presence of cytopathic
156 effect (CPE) was recorded (**Supplementary Fig 1A**) and titers were expressed
157 as the 50% tissue culture infectious dose (TCID₅₀), using the Reed-Muench

158 method. All experiments involving SARS-CoV-2 propagation were done in
159 biosafety level 3 laboratory.

160

161 ***In vitro* infection of PBMCs.** For these experiments, 10^6 PBMCs from 5
162 healthy donors were infected with SARS-CoV-2 (MOI=1) in RPMI with 0% FBS
163 at RT for 1 h under orbital agitation. Next, cells were pelleted at $300 \times g$, the
164 inoculum was washed and replaced by RPMI with 2% FBS and cells were
165 incubated at 37°C in 5% CO_2 . As controls, equivalent quantities of cells were
166 exposed to UV-inactivated SARS-CoV-2 and treated in the same way. We also
167 used a control consisting of cells treated with 20 mM of NH_4Cl starting 20 min
168 before infection and maintained throughout the entire incubation period.
169 Supernatants from PBMCs were collected at 0, 6, 12, 24 and 48 h post-infection
170 and subjected to serial ten-fold dilutions to determine virus titers by TCID_{50} , as
171 previously described. In parallel, PBMCs were treated with 0.5ug/ml Camostat
172 (Sigma Aldrich, cat. SML005) or with 10 μM of anti-ACE2 antibody (Rhea
173 Biotech, cat. IM-0060) starting 1 hour before infection. Then, inoculum was
174 washed, the media containing the different treatments were replaced, and the
175 PBMCs were kept for 24h at 37°C in 5% CO_2 .

176

177 **RNA extraction and real-time RT-PCR.** SARS-CoV-2 RNA detection was
178 done with primer-probe sets for SARS-CoV-2 according to the USA-CDC
179 protocol, targeting the virus N1 gene, and using the RNase-P housekeeping
180 gene as control, by one-step real-time RT-PCR. Total RNA was extracted with
181 Trizol® (Invitrogen, CA, EUA) from 250 μL of homogenized cell pellets and
182 supernatants from in vitro assays. All real-time PCR assays were done on a
183 Step-One Plus thermocycler (Applied Biosystems, Foster City, CA, USA).
184 Briefly, after Trizol® extraction, 100 ng of RNA was used for genome
185 amplification with N1 primers (20 μM) and probe (5 μM), and TaqPath 1-Step
186 qRT-PCR Master Mix (Applied Biosystems, Foster City, CA, USA), with the
187 following parameters: 25°C for 2 min, 50°C for 15 min, 95°C for 2 min, followed
188 by 45 cycles of 94°C for 5 s and 60°C for 30s. Viral loads of SARS-COV-2 were
189 determined using a standard curve prepared with a plasmid containing a 944bp
190 amplicon, which includes all three targets for the sets of primers/probes
191 designed by CDC protocol (N1, N2 and N3), inserted into a TA cloning vector

192 (PTZ57R/T CloneJet™ Cloning Kit Thermo Fisher®). Results of viral RNA
193 quantifications by one-step qRT-PCR were plotted with GraphPad® Prism 8.4.2
194 software.

195

196 **Indirect immunofluorescence staining of SARS-CoV-2 infected cells.**

197 Coverslips pre-treated with poly-lysine 0.1% (Sigma-Aldrich, cat. P8920) were
198 incubated with isolated PBMCs from patients or healthy donors at 37°C, 20
199 minutes for cell adherence. After that, coverslip-containing cells were fixed with
200 4% paraformaldehyde (PFA) in PBS for 15 minutes, and then washed 3 times
201 with PBS. To detect viral antigens in cells, we used serum from a recovered
202 COVID-19 patient, which was first tested for specificity by immunofluorescence
203 in SARS-CoV-2 infected Vero CCL81 cells (**Supplementary Fig 1B**). In
204 addition, for each experiment using the referred serum we included cells from
205 healthy donors or non-infected cells. As an isotype control of this serum, we
206 used a human serum collected in 2016. Biotin-conjugated anti-human IgG
207 (Sigma-Aldrich, cat. B-1140) was used as the secondary antibody, followed by
208 amplification with the TSA Cyanine 3 System (Perkin Elmer, NEL704A001KT),
209 following the manufacturer's protocol. To determine the phenotype of SARS-
210 CoV-2-infected cells, we used primary antibodies for CD4 (Abcam cat.
211 ab133616), CD8 (Abcam cat. ab4055), CD14 (Abcam cat. ab133335), CD19
212 (Abcam cat. ab134114), CD20 (Abcam cat. ab103573). For detection of virus
213 replication, we used a mouse anti-dsRNA J2 (dsRNA; English & Scientific
214 Consulting Kft, Hungary), which binds to dsRNA of 40 bp or longer. Secondary
215 antibodies used were polyclonal anti-rabbit conjugated with 488 (Thermo Fisher
216 cat. A21202), 594 (Abcam cat. ab150116) or 647 (Abcam cat. ab150079). The
217 Golgi complex and nuclei staining were carried out using a mouse anti-GM130
218 (BD cat. 610822) and 4',6-diamidino-2-phenylindole dihydrochloride dye (DAPI,
219 Thermo Fisher cat. 62248), respectively.

220

221 **Confocal microscopy.** PBMCs from confirmed COVID-19 patients and from
222 healthy control donors were stained with human serum containing antibodies to
223 SARS-CoV-2, and with commercial antibodies to the different cell phenotypes,
224 followed by the appropriate secondary antibodies. Preparations were analyzed
225 in a Zeiss Confocal 780 microscope in a Tile 3x3 in a single focal plane. The

226 quantity of SARS-CoV-2-positive cells of different phenotypes was quantified by
227 using the analyze particles tool from Fiji by ImageJ.

228

229 **Flow cytometry.** Unseparated whole blood leukocyte samples from COVID-19
230 patients or healthy donors infected in vitro with SARS-CoV-2 were surface
231 stained with Fixable Viability Dye eFluor™ 780 (eBioscience) and monoclonal
232 antibodies specific for CD3 (APC eBioscience cat. 17-0036-42), CD4 (PerCP-
233 Cy5.5 BD cat. 560650), CD8 (PE-Cy7 BD cat. 557746), CD19 (APC BioLegend
234 cat. 302212), CD14 (PerCP Abcam cat. ab91146), CD16 (PE eBioscience cat.
235 12-0168-42), CCR2 (BV BioLegend cat. 357210) for 30 min at 4°C, according to
236 manufacturer's instructions. Detection of SARS-CoV-2 by flow cytometry was
237 performed with BD Cytotfix/Cytoperm™ kit to enable access to intracellular
238 antigens using mouse polyclonal antibody raised against formalin-inactivated
239 SARS-CoV-2, as described early in this manuscript, for 15 min at 4°C. To
240 ensure that viral detection was specific for replicating intracellular viruses,
241 additional preparations of infected cells were stained without permeabilization.
242 Treatment with trypsin for 60 min on ice after infection to remove surface-bound
243 viral particles was also included as a second control (**Supplementary Fig 2**).
244 SARS-CoV-2 antibodies were detected with secondary anti-Mouse Alexa488.
245 Surface phosphatidylserine (PS) staining was carried out in whole blood using
246 ApoScreen AnnexinV-FITC apoptosis kit (SouthernBiotech cat 10010-02),
247 following manufacturer's guidelines. All data were acquired using a Verse or
248 Canto flow cytometers (BD Biosciences) and subsequent analysis was done
249 using FlowJo (TreeStar) software. Gating strategies are illustrated in
250 **Supplementary Fig 3**.

251

252 **Serial immunohistochemistry.** Tissue sections from paraffin-embedded lung
253 fragments obtained from two COVID-19 fatal cases were tested by
254 immunohistochemistry (IHC) using anti-SARS-CoV-2 polyclonal antibody for in
255 situ detection of SARS-CoV-2. Sequential immunoperoxidase labeling and
256 erasing (SIMPLE) [12] was then performed to determine the
257 immunophenotypes of SARS-CoV-2 infected cells, using antibodies to CD4
258 (Abcam cat. ab133616), CD20 (Abcam cat. ab103573), CD14 (Abcam cat.
259 ab133335) and IL-6 (BD cat. 554400). After each round of staining, slides were

260 scanned using a VS120 ScanScope (Olympus) under 400x magnification.
261 Images were pseudocolored and overlaid in the first image of the preparation
262 counterstained with hematoxylin using ImageJ v1.50b (NIH, USA) and Adobe
263 Photoshop CS5 software (Adobe Systems, San Jose, CA, USA). Lung paraffin-
264 embedded tissue obtained from a fatal case of hantavirus infection in 2016 was
265 used as a negative control for SARS-CoV-2 staining.

266

267 **Statistical analysis.** All descriptive statistics, patient stratification, and positive
268 cell frequencies were done using GraphPad Prism Software, version 6.0.
269 Correlation analysis, one-way ANOVA, two-way ANOVA, linear regressions,
270 Holm-Sidak, and Bonferroni post-tests were also performed using GraphPad
271 Prism. Values of $P < 0.05$ were considered significant, as described in all
272 figures.

273

274

275 **Results**

276

277 **SARS-CoV-2 infection of human PBMCs is productive.** Considering that
278 human lymphocyte and monocyte lineages are susceptible to SARS-CoV-2
279 infection *in vitro*, we sought to determine whether primary cultures of human
280 PBMCs could also be infected. Therefore, PBMCs from five healthy donors
281 were infected *in vitro* at a MOI=1. After 0, 6, 12, 24 and 48 hpi, supernatants
282 were harvested, and virus progeny was titrated. SARS-CoV-2 titers peaked
283 between 6 and 12 hpi, resulting in a 100-fold increase from the initial input, and
284 decreased steadily thereof (**Fig 1A**). As expected, induction of general
285 intracellular alkalization by treatment with NH₄Cl reduced progeny production by
286 approximately 10x (p=0.017). Interestingly, virus progeny production was not
287 entirely abolished by NH₄Cl treatment, suggesting an entry pathway alternative
288 to endosomal acidification in PBMCs (**Fig 1B**).

289 Even though expression of ACE2 is minimal in human PBMCs in general
290 [13, 14], we evaluated the viral production after blocking ACE2 and TMPRSS2.
291 Virus titers obtained after Camostat blockage of TMPRSS2 were not
292 significantly different from those obtained without the treatment (**Fig 1C**),
293 suggesting that PBMC infection is not dependent on TMPRSS2. Conversely,
294 the blockage of ACE2 with anti-ACE2 antibody resulted in reduction, but not
295 abrogation of SARS-CoV-2 progeny production after 24 hpi (p=0.0216) (**Fig**
296 **1C**), indicating that SARS-CoV-2 can infect human PBMCs independently of
297 ACE2.

298 Coronavirus replication entails the formation of abundant double-
299 stranded RNAs (dsRNA) in the cytoplasm of infected cells, and thus its
300 intracellular detection is a reliable marker of viral replication. Therefore, infected
301 PBMCs were stained for SARS-CoV-2 and dsRNA and analyzed by confocal
302 microscopy. Most SARS-CoV-2-positive cells were also positive for dsRNA, and
303 rates of double-positive cells counted at 6 hours post-infection followed a
304 pattern that roughly matched the accumulation of progeny (**Fig. 1D**). The
305 dsRNA staining was seen as clear puncta in SARS-CoV-2-infected cells, in a
306 pattern suggestive of virus factories.

307

308 **Monocytes and T lymphocytes are the main targets of SARS-CoV-2 in**
309 ***vitro* infection.** To determine the susceptibility of circulating leukocytes to
310 SARS-CoV-2, PBMCs from five healthy donors were infected (MOI=1), and
311 analyzed the intracellular expression of SARS-CoV-2 antigens by flow
312 cytometry. After 24 hpi, SARS-CoV-2 was detected in all immunophenotyped
313 cells (**Fig 2A**). Monocytes were the most susceptible cell type, showing
314 significant SARS-CoV-2 antigen staining (44.3%, $p=0.039$) (**Fig 2B**). In addition
315 to monocytes, T CD4⁺ (14.2%, $p=0.028$), CD8⁺ (13.5%, $p=0.019$) and B
316 lymphocytes (7.58%) were also susceptible to SARS-2 infection (**Fig 2C**).
317 Staining for SARS-CoV-2 was significantly reduced in cells treated with NH₄Cl,
318 suggesting that acidification is important for *in vitro* infection of PBMCs.

319

320 **Infection of T lymphocytes leads to cell death by apoptosis.** The COVID-
321 19-related lymphocytopenia has been well described as a strong indicator of
322 severe clinical outcomes in patients. Since we found both T CD4⁺ and CD8⁺
323 cells susceptible to SARS-2 infection *in vitro*, we investigated the presence of
324 cell death in SARS-CoV-2-infected PBMCs from 5 healthy donors by the
325 expression of translocated phosphatidylserine (PS) on the cell surface 24 hours
326 post-infection by analyzing its binding to annexin V (**Fig 3**). Despite the basal
327 annexin V staining (CD4⁺ mean 6.24%, CD8⁺ mean 12.36%) seen in non-
328 infected cells (**Fig 3A**), strong staining was observed both in live T CD4⁺
329 (70.88%, $p=0.0001$) and CD8⁺ lymphocytes (39.72%, $p=0.0009$) (**Fig 3B**).
330 When cells were analyzed independently of Live/Dead staining, differences
331 were still significant and even increased for CD8⁺ (59.64%, $p=0.0001$)
332 (**Supplementary Fig 4**), indicating that a considerable percentage of Annexin
333 V-positive CD8⁺ cells were already dead. No significant differences were
334 observed in cell death between cells infected in the presence or absence of
335 NH₄Cl during infection. These results indicated that infection of human PBMCs
336 by SARS-CoV-2 sharply increased the expression of apoptosis markers in T
337 lymphocytes.

338

339 **Circulating immune cells from COVID-19 patients are infected by SARS-**
340 **CoV-2.** During April 7th to June 18th, we enrolled 22 COVID-19 patients that
341 were admitted to the intensive care unit (ICU), presenting a moderate to severe

342 disease. Clinical and demographic characteristics of enrolled patients are listed
343 in Supplementary Table 1. Blood samples were collected at admission in the
344 ICU. To check for SARS-CoV-2 infection in PBMCs from COVID patients, we
345 analyzed PBMCs prepared from the whole blood of 22 patients and 11 healthy
346 donors by flow cytometry (**Fig 4A**) with staining for SARS-CoV-2 antigens. Cells
347 from COVID-19 patients showed significant expression of SARS-CoV-2
348 antigens ($7.68\% \pm 1.56$ $p=0.008$) in comparison with cells from healthy donors
349 (**Fig 4B**). Interestingly, not all COVID-19 patients showed expressive staining
350 for SARS-CoV-2, and rates of SARS-CoV-2-positive cells ranged from 0.16 to
351 33.9% (**Fig 4B**). Additionally, PMBCs from 15 COVID-19 patients were tested
352 for the SARS-CoV-2 genome by real-time RT-PCR. Viral genome was detected
353 in 8 out of 15 PBMC samples (53.3%), with mean viral load of 3.8×10^4 copies
354 per μg of RNA (**Supplementary Table 2**). Immunophenotyping of cells from
355 COVID-19 patients indicated that the highest proportion of SARS-CoV-2-
356 positive cells was found in B lymphocytes ($42.73\% \pm 4.3$). Although susceptible
357 to *in vitro* infection, we were not able to find significant numbers of SARS-CoV-2
358 positive T cells in PBMCs from COVID-19 patients by flow cytometry. Similarly
359 to what was observed by the *in vitro* experiments, monocytes (CD14^+) from
360 patients were found to be positive for SARS-CoV-2 in a high percentage
361 ($14.19\% \pm 15.26$). Inflammatory monocytes ($\text{CD14}^+\text{CCR2}^+$ and
362 $\text{CD14}^+\text{CD16}^+\text{CCR2}^+$) were positive for SARS-CoV-2 antigen in rates
363 significantly higher in comparison with healthy controls ($18.73\% \pm 18.46$ and
364 $14.78\% \pm 15.5$, respectively) (**Fig 4C**). To confirm the results obtained by flow
365 cytometry, immunofluorescence was done for SARS-CoV-2 antigens in PBMCs
366 isolated from COVID-19 patients. Some staining of SARS-CoV-2 with variable
367 intensity was observed in CD19 and CD14 cells in PBMCs from COVID-19
368 patients, with no discernible fluorescent signal seen in PBMCs from healthy
369 donors (**Fig 4D**). Despite what was observed by FC experiments, some IF
370 staining was found in CD4 T lymphocytes, and after extensively screening, very
371 few T CD8 cells were found to be positive for IF (**Supplementary Fig 5**).

372 Since the detection of SARS-CoV-2 in patients was found to be variable
373 (Figure 4C), we selected 15 COVID cases to analyze individual differences in
374 rates of SARS-CoV-2-positive cells. Patients were stratified based on the time
375 of sample collection after symptoms onset, and SARS-CoV-2-positive cell

376 frequencies were plotted on a heatmap for all cell immunophenotypes analyzed
377 (**Fig 4E**). It became clear that rates of SARS-CoV-2-positive B lymphocytes
378 were high throughout the entire dataset. In contrast, rates of SARS-CoV-2-
379 positive monocytes were higher after following time progression after symptoms
380 onset (**Fig 4E**). Frequencies of SARS-CoV-2-positive cells correlated positively
381 with the length of time of COVID-19 progression after symptoms onset,
382 especially for inflammatory CD14⁺CCR2⁺ monocytes ($r=0.442$ $p=0.044$) (**Fig**
383 **4F**).

384 To confirm whether SARS-CoV-2 was actively replicating in PBMCs from
385 COVID-19 patients, we analyzed the presence of dsRNA in SARS-CoV-2-
386 positive cells of different immunophenotypes by immunofluorescence and
387 confocal microscopy. Remarkably, dsRNA staining was found in most SARS-
388 CoV-2-positive cell subsets, CD4⁺ T lymphocytes, B lymphocytes, and
389 monocytes (**Fig 5**). Altogether, these data confirm that SARS-CoV-2 infects
390 circulating white blood cells from COVID-19 patients, and the frequencies of
391 SARS-CoV-2-positive monocytes in the peripheral blood increase with time of
392 onset of symptoms.

393

394 **Infected inflammatory monocytes are detected post mortem in lung**
395 **tissues from COVID-19 patients.** The respiratory tract is the classical entry
396 route of coronaviruses in mammalian hosts. Therefore, we checked if the same
397 infected cell immunophenotypes found in PBMCs could also be found by
398 immunohistochemistry in the lungs of COVID-19 patients obtained *post mortem*.
399 Post mortem lung specimens from COVID-19 patients revealed abundant
400 staining for SARS-CoV-2, especially throughout the entire bronchovascular
401 axes and alveolar-capillary barriers. Control lung specimens showed no staining
402 (**Supplementary Fig 6**). Upon staining for SARS-CoV-2, slides were scanned,
403 the staining was erased, and re-stained sequentially for the surface antigens
404 CD4, CD20, and CD14. The serial immunolabelling indicated that CD4⁺ T
405 lymphocytes, B lymphocytes, and monocytes express SARS-CoV-2 antigens
406 (**Fig 6**) in the lungs of COVID-19 cases. Additionally, due to its well-known role
407 in lung tissue damage in COVID-19, IL-6-positive cells were also searched for
408 and, interestingly, several CD14⁺ monocytes expressing IL-6 were also positive

409 for SARS-CoV-2 (**Fig 6C-E**), indicating that inflammatory monocytes in lungs of
410 COVID-19 patients can also be infected with SARS-CoV-2.

411

412 **Discussion**

413

414 It has been well accepted that several SARS-CoV-2 strategies to escape
415 innate immune sensing, coupled with dysregulation of immune responses in
416 early phases of infection, drive a cytokine storm that is a hallmark of severe
417 COVID-19 [15–17]. Importantly, lymphopenia has also been recognized as a
418 feature of severe infection by SARS-CoV-2. Postmortem examination of
419 spleens and lymph nodes showed the presence of SARS-CoV-2 in those
420 organs, infecting ACE2-expressing macrophages and causing important tissue
421 damage [10].

422 SARS-CoV-2 detection in tissues far from the entry sites in the
423 respiratory tract, without exuberant viremia, suggests that SARS-CoV-2 may
424 reach target organs by alternative ways. One possibility could be the infection of
425 leukocytes that could serve as "Trojan horses" transporting the virus to
426 secondary infection sites. In that regard, we have recently reported that SARS-
427 CoV-2 infects neutrophils, which could also act as Trojan horses carrying
428 SARS-CoV-2 to neutrophil infiltrated tissues [18]. However, until now, it has
429 been unclear whether SARS-CoV-2 infects PBMCs *in vivo*, thus creating a
430 possibility of them being Trojan horses of viral dissemination. To address this
431 question, we first infected PBMCs from healthy donors *in vitro* with SARS-CoV-
432 2, as a preliminary way to check for their susceptibility and permissiveness to
433 the virus. Virus production in PBMCs peaked at 12 hpi, reaching titers 100-fold
434 the initial input, with steady decay thereafter until 48 hpi. The presence of
435 dsRNA in SARS-CoV-2 infected PBMCs in the first few hours after infection
436 provides further evidence that the virus replicates, yet modestly, in PBMCs *in*
437 *vitro*. These results are in keeping with reports of SARS-CoV infection of human
438 PBMCs [19]. Moreover, the treatment of PBMCs with ammonium chloride,
439 which elevates the pH and prevents organelle acidification, significantly reduced
440 but did not abrogate SARS-CoV-2 replication, consistent with an alternative
441 acidification-independent pathway.

442 The immunophenotyping of PBMCs infected in vitro with SARS-CoV-2
443 revealed that CD14⁺, CD4⁺, CD8⁺ and CD19⁺ cells were susceptible. Primary
444 human monocytes have been reported as susceptible to MERS-CoV and, more
445 recently, to SARS-CoV-2 [20, 21]. In contrast, another recent study did not
446 report PBMC infection by SARS-CoV-2 in vitro, possibly due to the low MOI
447 used [22], coupled with the reported reduced expression of ACE2 by
448 lymphocytes [14]. Despite that, we found that blockade of ACE2 partially
449 reduced SARS-CoV-2 titers in supernatants of infected PBMCs, suggesting that
450 among PBMCs there are ACE2-expressing cell types that contribute to the total
451 virus progeny production. However, ACE2 blockade does not eliminate virus
452 production, what strongly suggests the existence of ACE2-independent
453 mechanisms of infection in lymphohematopoietic cells.

454 A recent report indicated that SARS-CoV-2 spike protein can interact
455 with surface CD147, which could be an alternative virus receptor, in a way
456 similar to what was observed for SARS-CoV [7, 23]. The transmembrane
457 glycoprotein CD147, also known as Basigin, is expressed in some subsets of
458 T lymphocytes [24], and thus could play a role in SARS-CoV-2 entry in these
459 cells as well.

460 An intense T cell depletion in peripheral blood is seen in up to 85% of
461 severe COVID-19 patients [2, 25]. Furthermore, T cells from COVID-19 patients
462 show considerable levels of exhaustion markers [3, 4], and transcriptome
463 analysis of their PBMCs indicated upregulation of genes involved in apoptosis
464 and p53-signalling pathways [5]. These data suggests that SARS-CoV-2
465 infection could induce cell death by apoptosis in PBMCs, what could also
466 happen in inflamed secondarily infected organs of COVID-19 patients. Of note,
467 lymphopenia was also described in Middle East Respiratory Syndrome (MERS)
468 patients, in whom MERS-CoV can directly infect human primary T lymphocytes
469 and induce T-cell apoptosis through extrinsic and intrinsic pathways [20].

470 Annexin V staining showed that SARS-CoV-2 infection of PBMCs caused
471 increased translocation of phosphatidylserine (PS) to the cell surface of both
472 CD4⁺ and CD8⁺ T lymphocytes. The translocation of PS and subsequent
473 scrambling of lipid membrane asymmetry is indicative of late-stage apoptosis
474 [26]. Importantly, in the presence of NH₄Cl, SARS-CoV-2 infection significantly
475 increased annexin V labelling, suggesting that even at reduced levels of

476 replication, SARS-CoV-2 can trigger apoptosis in lymphocytes. Taken together,
477 the data indicate that SARS-CoV-2 infection of lymphocytes causes cell death,
478 which may concur to the observed lymphopenia. The association of
479 lymphopenia with poor prognosis may be related to the death of specific T-cell
480 subsets, which may result in loss of immune response regulatory components,
481 and drive a cytokine storm that can crosstalk with neutrophil NETosis [27]. Also,
482 it can be related to increased IL-6 and Fas-FasL interactions [10], resulting in
483 severe lymphoid tissue alterations [28].

484 In addition to *in vitro* infection, SARS-CoV-2 was also detected in PBMCs
485 from COVID-19 patients, more prominently in B lymphocytes and
486 subpopulations of monocytes. The predominance of B lymphocytes as target
487 cells of SARS-CoV-2 infection *in vivo*, in contrast to what was seen in PBMCs
488 infected *in vitro*, suggests that the susceptibility of different lymphocyte subsets
489 in natural SARS-CoV-2 infection may depend on ACE2-independent alternative
490 virus entry mechanisms. These findings corroborate previous observations that
491 SARS-CoV enters B lymphocytes and monocyte-derived cells via a FcγRII-
492 dependent pathway, which is facilitated by the presence of antibodies [29, 30].
493 The present results were obtained based on one-time sampling of patients who
494 were enrolled at different times of COVID-19 evolution, what may explain the
495 heterogeneity in rates of SARS-CoV-2-positive cells of different
496 immunophenotypes observed among them. Accordingly, SARS-CoV-2 RNA
497 was not detected in PBMCs from all, but in 53% of patients, indicating that
498 SARS-CoV-2 infection in PBMCs may be variable, depending on host factors
499 still unidentified, or present only in later phases of COVID-19, as suggested by
500 the positive correlation between time from symptoms onset and frequency of
501 SARS-CoV-2 positive cells in PBMCs. A possible explanation for an increase in
502 SARS-CoV-2 susceptible cells over time could be an increase in ACE2
503 expression, triggered by type I IFN [31]. In this context, it is noteworthy that the
504 replication of SARS-CoV in PBMCs was not sustained for long periods [19, 32].

505 To the best of our knowledge, this is the first report of circulating
506 lymphoid cells positive for SARS-CoV-2, and the presence of dsRNA indicates
507 that these cells are targets of virus replication. This may considerably impact
508 the cells immune competence during COVID-19 and may help cell-associated
509 SARS-CoV-2 spread to secondary infection sites.

510 SARS-CoV-2 recruits important inflammatory infiltrate in the lungs,
511 containing diverse immune cell types that bear close contact with SARS-CoV-2-
512 infected lung cells, such as pneumocytes and alveolar macrophages [33]. In the
513 present study, we found CD4⁺ T and B lymphocytes and, importantly, also IL-6-
514 expressing inflammatory monocytes positive for SARS-CoV-2 infiltrating the
515 lung tissue from fatal cases of COVID-19. Further studies will be required to
516 clarify whether SARS-CoV-2-positive lympho-mononuclear cells become
517 infected in the lung or enter the affected tissue from the bloodstream already
518 containing the virus. Regardless of where the immune cells become infected by
519 SARS-CoV-2, their presence in the peripheral blood can impact directly on virus
520 dissemination, delivering the infectious virus to secondary sites of infection.

521 Inflammatory monocytes play a significant role in the immunopathology
522 of COVID-19 [15, 16] and ICU patients have high levels of circulating
523 CD14⁺CD16⁺ inflammatory monocytes, which correlates with unfavorable
524 outcomes [34, 35]. Increased expression of CCR2 and other inflammatory
525 markers by monocytes leads to the infiltration of tissues with high expression of
526 the correspondent CCL2 chemokine [15]. Interestingly, inflammatory monocytes
527 with the same profile were found abundantly in bronchoalveolar lavage fluids
528 from patients with severe COVID-19 [36]. Based on that, our data suggest that
529 CD14⁺CCR2⁺ and CD14⁺CD16⁺CCR2⁺ infected monocytes could act as
530 Trojan horses and traffic viruses to secondary sites of infection, where SARS-
531 CoV-2 causes severe tissue damage. Additional lymphoid cell recruitment to
532 damaged tissues may further contribute to lymphopenia [9].

533 Overall, the infection of lymphomononuclear cells by SARS-CoV-2 in
534 peripheral blood from patients with COVID-19 has important consequences for
535 pathogenesis of this multifaceted disease, including possible compromises of
536 immune cell functions, and helping the virus to reach immune-privileged
537 secondary sites of infection.

538

539 **Conflict of interests**

540 The authors declare none.

541

542 **Acknowledgements**

543 This study was supported by the Brazilian National Research Council
544 (CNPq grant numbers 310100/2017-8, 403201/2020-9 and INCTC
545 465539/2014-9) and the Sao Paulo State Research Foundation (FAPESP grant
546 numbers 2013/16349-2 and 2014/02438-6). Dr. Pontelli was funded by CNPq
547 grant number 380849/2020-8. The authors also thank Dimensions Sciences, a
548 Non-Profit Organization that granted Dr. Castro a research scholarship while
549 this study was conducted.

550

551

552

553

554

References

555

556 [1] Zhou, P.; Yang, X. Lou; Wang, X. G.; Hu, B.; Zhang, L.; Zhang, W.; Si, H. R.; Zhu, Y.; Li,
557 B.; Huang, C. L.; et al. A Pneumonia Outbreak Associated with a New Coronavirus of
558 Probable Bat Origin. *Nature*, **2020**, *579* (7798), 270–273. [https://doi.org/10.1038/s41586-](https://doi.org/10.1038/s41586-020-2012-7)
559 020-2012-7.

560 [2] Huang, C.; Wang, Y.; Li, X.; Ren, L.; Zhao, J.; Hu, Y.; Zhang, L.; Fan, G.; Xu, J.; Gu, X.;
561 et al. Clinical Features of Patients Infected with 2019 Novel Coronavirus in Wuhan,
562 China. *Lancet*, **2020**, *395* (10223), 497–506. [https://doi.org/10.1016/S0140-](https://doi.org/10.1016/S0140-6736(20)30183-5)
563 6736(20)30183-5.

564 [3] Diao, B.; Wang, C.; Tan, Y.; Chen, X.; Liu, Y.; Ning, L.; Chen, L.; Li, M.; Liu, Y.; Wang,
565 G.; et al. Reduction and Functional Exhaustion of T Cells in Patients With Coronavirus
566 Disease 2019 (COVID-19). *Front. Immunol.*, **2020**, *11* (May), 1–7.
567 <https://doi.org/10.3389/fimmu.2020.00827>.

568 [4] Zheng, H. Y.; Zhang, M.; Yang, C. X.; Zhang, N.; Wang, X. C.; Yang, X. P.; Dong, X. Q.;
569 Zheng, Y. T. Elevated Exhaustion Levels and Reduced Functional Diversity of T Cells in
570 Peripheral Blood May Predict Severe Progression in COVID-19 Patients. *Cell. Mol.*
571 *Immunol.*, **2020**, *17* (5), 541–543. <https://doi.org/10.1038/s41423-020-0401-3>.

572 [5] Xiong, Y.; Liu, Y.; Cao, L.; Wang, D.; Guo, M.; Jiang, A.; Guo, D.; Hu, W.; Yang, J.;
573 Tang, Z.; et al. Transcriptomic Characteristics of Bronchoalveolar Lavage Fluid and
574 Peripheral Blood Mononuclear Cells in COVID-19 Patients. *Emerg. Microbes Infect.*,
575 **2020**, *9* (1), 761–770. <https://doi.org/10.1080/22221751.2020.1747363>.

576 [6] Hoffmann, M.; Kleine-Weber, H.; Schroeder, S.; Kruger, N.; Herrler, T.; Erichsen, S.;
577 Schiergens, T. S.; Wu, N.-H.; Nitsche, A.; Muller, M. A.; et al. SARS-CoV-2 Cell Entry
578 Depends on ACE2 and TMPRSS2 and Is Blocked by a Clinically Proven Protease
579 Inhibitor. *Cell*, **2020**, *181* (16), 1–9.

580 [7] Wang, K.; Chen, W.; Chen, Z.-N. SARS-CoV-2 Invades Host Cells via a Novel Route:
581 CD147-Spike Protein. *bioRxiv*, **2012**, *91* (5), 1–10.
582 <https://doi.org/10.1101/2020.03.14.988345>.

583 [8] Zang, R.; Gomez Castro, M. F.; McCune, B. T.; Zeng, Q.; Rothlauf, P. W.; Sonnek, N.
584 M.; Liu, Z.; Brulois, K. F.; Wang, X.; Greenberg, H. B.; et al. TMPRSS2 and TMPRSS4
585 Promote SARS-CoV-2 Infection of Human Small Intestinal Enterocytes. *Sci. Immunol.*,
586 **2020**, *5* (47). <https://doi.org/10.1126/sciimmunol.abc3582>.

587 [9] chen, yongwen; Feng, Z.; Diao, B.; Wang, R.; Wang, G.; Wang, C.; Tan, Y.; Liu, L.;
588 Wang, C.; Liu, Y.; et al. The Novel Severe Acute Respiratory Syndrome Coronavirus 2
589 (SARS-CoV-2) Directly Decimates Human Spleens and Lymph Nodes. *medRxiv*, **2020**,
590 *2*, 2020.03.27.20045427. <https://doi.org/10.1101/2020.03.27.20045427>.

591 [10] Rios-Santos, F.; Alves-Filho, J. C.; Souto, F. O.; Spiller, F.; Freitas, A.; Lotufo, C. M. C.;
592 Soares, M. B. P.; Dos Santos, R. R.; Teixeira, M. M.; Cunha, F. D. Q. Down-Regulation
593 of CXCR2 on Neutrophils in Severe Sepsis Is Mediated by Inducible Nitric Oxide

- 594 Synthase-Derived Nitric Oxide. *Am. J. Respir. Crit. Care Med.*, **2007**, 175 (5), 490–497.
595 <https://doi.org/10.1164/rccm.200601-103OC>.
- 596 [11] Alves-Filho, J. C.; Freitas, A.; Souto, F. O.; Spiller, F.; Paula-Neto, H.; Silva, J. S.;
597 Gazzinelli, R. T.; Teixeira, M. M.; Ferreira, S. H.; Cunha, F. Q. Regulation of Chemokine
598 Receptor by Toll-like Receptor 2 Is Critical to Neutrophil Migration and Resistance to
599 Polymicrobial Sepsis. *Proc. Natl. Acad. Sci. U. S. A.*, **2009**, 106 (10), 4018–4023.
600 <https://doi.org/10.1073/pnas.0900196106>.
- 601 [12] Glass, G.; Papin, J. A.; Mandell, J. W. SIMPLE: A Sequential Immunoperoxidase
602 Labeling and Erasing Method. *J. Histochem. Cytochem.*, **2009**, 57 (10), 899–905.
603 <https://doi.org/10.1369/jhc.2009.953612>.
- 604 [13] Qi, F.; Qian, S.; Zhang, S.; Zhang, Z. Single Cell RNA Sequencing of 13 Human Tissues
605 Identify Cell Types and Receptors of Human Coronaviruses. *Biochem. Biophys. Res.*
606 *Commun.*, **2020**, 526 (1), 135–140. <https://doi.org/10.1016/j.bbrc.2020.03.044>.
- 607 [14] Uhlén, M.; Fagerberg, L.; Hallström, B. M.; Lindskog, C.; Oksvold, P.; Mardinoglu, A.;
608 Sivertsson, Å.; Kampf, C.; Sjöstedt, E.; Asplund, A.; et al. Tissue-Based Map of the
609 Human Proteome. *Science (80-.)*, **2015**, 347 (6220).
610 <https://doi.org/10.1126/science.1260419>.
- 611 [15] Zhou, Y.; Fu, B.; Zheng, X.; Wang, D.; Zhao, C.; Qi, Y.; Sun, R.; Tian, Z.; Xu, X.; Wei, H.
612 Pathogenic T-Cells and Inflammatory Monocytes Incite Inflammatory Storms in Severe
613 COVID-19 Patients. *Natl. Sci. Rev.*, **2020**, No. March, 1–5.
614 <https://doi.org/10.1093/nsr/nwaa041>.
- 615 [16] Mehta, P.; McAuley, D. F.; Brown, M.; Sanchez, E.; Tattersall, R. S.; Manson, J. J.
616 COVID-19: Consider Cytokine Storm Syndromes and Immunosuppression. *Lancet*,
617 **2020**, 395 (10229), 1033–1034. [https://doi.org/10.1016/S0140-6736\(20\)30628-0](https://doi.org/10.1016/S0140-6736(20)30628-0).
- 618 [17] Vabret, N.; Britton, G. J.; Gruber, C.; Hegde, S.; Kim, J.; Kuksin, M.; Levantovsky, R.;
619 Malle, L.; Moreira, A.; Park, M. D.; et al. Immunology of COVID-19: Current State of the
620 Science. *Immunity*, **2020**, 1. <https://doi.org/10.1016/j.immuni.2020.05.002>.
- 621 [18] Veras, F.; Pontelli, M. C.; Cunha, F. SARS-CoV-2 Triggered Neutrophil Extracellular
622 Traps (NETs) Mediate COVID-19 Pathology. *medRxiv*, **2020**.
- 623 [19] Li, L.; Wo, J.; Shao, J.; Zhu, H.; Wu, N.; Li, M.; Yao, H.; Hu, M.; Dennin, R. H. SARS-
624 Coronavirus Replicates in Mononuclear Cells of Peripheral Blood (PBMCs) from SARS
625 Patients. *J. Clin. Virol.*, **2003**, 28 (3), 239–244. [https://doi.org/10.1016/S1386-6532\(03\)00195-1](https://doi.org/10.1016/S1386-6532(03)00195-1).
- 626
- 627 [20] Chu, H.; Zhou, J.; Wong, B. H. Y.; Li, C.; Chan, J. F. W.; Cheng, Z. S.; Yang, D.; Wang,
628 D.; Lee, A. C. Y.; Li, C.; et al. Middle East Respiratory Syndrome Coronavirus Efficiently
629 Infects Human Primary T Lymphocytes and Activates the Extrinsic and Intrinsic
630 Apoptosis Pathways. *J. Infect. Dis.*, **2016**, 213 (6), 904–914.
631 <https://doi.org/10.1093/infdis/jiv380>.
- 632 [21] Codo, A. C.; Davanzo, G. G.; Monteiro, L. D. B.; Souza, G. F. De; Muraro, S. P.;
633 Carregari, V. C.; Alberto, C.; Biagi, O. De; Crunfli, F.; Jimenez, J. L.; et al. Elevated

- 634 Glucose Levels Favor SARS-CoV-2 Infection and Monocyte Response through a HIF-
635 1 α /Glycolysis Dependent Axis.
- 636 [22] Banerjee, A.; Nasir, J. A.; Budyłowski, P.; Yip, L.; Aftanas, P.; Christie, N.; Ghalami, A.;
637 Baid, K.; Raphenya, A. R.; Hirota, J. A.; et al. Isolation, Sequence, Infectivity, and
638 Replication Kinetics of Severe Acute Respiratory Syndrome Coronavirus 2. *Emerg.*
639 *Infect. Dis.*, **2020**, 26 (9). <https://doi.org/10.3201/eid2609.201495>.
- 640 [23] Chen, Z.; Mi, L.; Xu, J.; Yu, J.; Wang, X.; Jiang, J.; Xing, J.; Shang, P.; Qian, A.; Li, Y.; et
641 al. Function of HAb18G/CD147 in Invasion of Host Cells by Severe Acute Respiratory
642 Syndrome Coronavirus. *J. Infect. Dis.*, **2005**, 191 (5), 755–760.
643 <https://doi.org/10.1086/427811>.
- 644 [24] Solstad, T.; Bains, S. J.; Landskron, J.; Aandahl, E. M.; Thiede, B.; Taskén, K.;
645 Torgersen, K. M. CD147 (Basigin/Emmprin) Identifies FoxP3 +CD45RO +CTLA4 +
646 Activated Human Regulatory T Cells. *Blood*, **2011**, 118 (19), 5141–5151.
647 <https://doi.org/10.1182/blood-2011-02-339242>.
- 648 [25] Chen, N.; Zhou, M.; Dong, X.; Qu, J.; Gong, F.; Han, Y.; Qiu, Y.; Wang, J.; Liu, Y.; Wei,
649 Y.; et al. Epidemiological and Clinical Characteristics of 99 Cases of 2019 Novel
650 Coronavirus Pneumonia in Wuhan, China: A Descriptive Study. *Lancet*, **2020**, 395
651 (10223), 507–513. [https://doi.org/10.1016/S0140-6736\(20\)30211-7](https://doi.org/10.1016/S0140-6736(20)30211-7).
- 652 [26] Suzuki, J.; Denning, D. P.; Imanishi, E.; Horvitz, H. R.; Nagata, S. Xk-Related Protein 8
653 and CED-8 Promote Phosphatidylserine Exposure in Apoptotic Cells. *Science (80-.)*,
654 **2013**, 341 (6144), 403–406. <https://doi.org/10.1126/science.1236758>.
- 655 [27] Barnes, B. J.; Adrover, J. M.; Baxter-Stoltzfus, A.; Borczuk, A.; Cools-Lartigue, J.;
656 Crawford, J. M.; Daßler-Plenker, J.; Guerci, P.; Huynh, C.; Knight, J. S.; et al. Targeting
657 Potential Drivers of COVID-19: Neutrophil Extracellular Traps. *J. Exp. Med.*, **2020**, 217
658 (6), 1–7. <https://doi.org/10.1084/jem.20200652>.
- 659 [28] Blanco-Melo, D.; Nilsson-Payant, B. E.; Liu, W. C.; Uhl, S.; Hoagland, D.; Møller, R.;
660 Jordan, T. X.; Oishi, K.; Panis, M.; Sachs, D.; et al. Imbalanced Host Response to
661 SARS-CoV-2 Drives Development of COVID-19. *Cell*, **2020**, 181 (5), 1036-1045.e9.
662 <https://doi.org/10.1016/j.cell.2020.04.026>.
- 663 [29] Kam, Y. W.; Kien, F.; Roberts, A.; Cheung, Y. C.; Lamirande, E. W.; Vogel, L.; Chu, S.
664 L.; Tse, J.; Guarner, J.; Zaki, S. R.; et al. Antibodies against Trimeric S Glycoprotein
665 Protect Hamsters against SARS-CoV Challenge despite Their Capacity to Mediate
666 FcyRII-Dependent Entry into B Cells in Vitro. *Vaccine*, **2007**, 25 (4), 729–740.
667 <https://doi.org/10.1016/j.vaccine.2006.08.011>.
- 668 [30] Jaume, M.; Yip, M. S.; Cheung, C. Y.; Leung, H. L.; Li, P. H.; Kien, F.; Dutry, I.;
669 Callendret, B.; Escriou, N.; Altmeyer, R.; et al. Anti-Severe Acute Respiratory Syndrome
670 Coronavirus Spike Antibodies Trigger Infection of Human Immune Cells via a PH- and
671 Cysteine Protease-Independent Fc R Pathway. *J. Virol.*, **2011**, 85 (20), 10582–10597.
672 <https://doi.org/10.1128/jvi.00671-11>.
- 673 [31] Ziegler, C. G. K.; Allon, S. J.; Nyquist, S. K.; Mbanjo, I. M.; Miao, V. N.; Tzouanas, C. N.;

- 674 Cao, Y.; Yousif, A. S.; Bals, J.; Hauser, B. M.; et al. SARS-CoV-2 Receptor ACE2 Is an
675 Interferon-Stimulated Gene in Human Airway Epithelial Cells and Is Detected in Specific
676 Cell Subsets across Tissues. *Cell*, **2020**, 1016–1035.
677 <https://doi.org/10.1016/j.cell.2020.04.035>.
- 678 [32] Yilla, M.; Harcourt, B. H.; Hickman, C. J.; McGrew, M.; Tamin, A.; Goldsmith, C. S.;
679 Bellini, W. J.; Anderson, L. J. SARS-Coronavirus Replication in Human Peripheral
680 Monocytes/Macrophages. *Virus Res.*, **2005**, 107 (1), 93–101.
681 <https://doi.org/10.1016/j.virusres.2004.09.004>.
- 682 [33] Roosecelis B. Martines; Ritter, J. M.; Matkovic, E.; Gary, J.; Bollweg, B. C.; Bullock, H.;
683 Goldsmith, C. S.; Silva-Flannery, L.; Seixas, J. N.; Reagan-Steiner, S.; et al. Pathology
684 and Pathogenesis of SARS-CoV-2 Associated with Fatal Coronavirus Disease, United
685 States. *Emerg. Infect. Dis.*, **2020**, 26. <https://doi.org/10.3201/eid2609.202095>.
- 686 [34] Zhang, D.; Guo, R.; Lei, L.; Liu, H.; Wang, Y.; Wang, Y.; Dai, T.; Zhang, T.; Lai, Y.;
687 Wang, J.; et al. COVID-19 Infection Induces Readily Detectable Morphological and
688 Inflammation-Related Phenotypic Changes in Peripheral Blood Monocytes, the Severity
689 of Which Correlate with Patient Outcome. *medRxiv*, **2020**, 2020.03.24.20042655.
690 <https://doi.org/10.1101/2020.03.24.20042655>.
- 691 [35] Zhou, Y.; Fu, B.; Zheng, X.; Wang, D.; Zhao, C. In Severe Pulmonary Syndrome
692 Patients of a New Coronavirus. **2020**.
- 693 [36] Liao, M.; Liu, Y.; Yuan, J.; Wen, Y.; Xu, G.; Zhao, J.; Cheng, L.; Li, J.; Wang, X.; Wang,
694 F.; et al. Single-Cell Landscape of Bronchoalveolar Immune Cells in Patients with
695 COVID-19. *Nat. Med.*, **2020**, 26 (6), 842–844. [https://doi.org/10.1038/s41591-020-0901-](https://doi.org/10.1038/s41591-020-0901-9)
696 9.
697
698

699 **Figure legends**

700

701 **Figure 1. Human primary blood cells are susceptible and permissive to**

702 **SARS-CoV-2.** Blood from five healthy donors was collected and PBMCs were
703 separated by Ficoll density gradient. Cells were infected with SARS-CoV-2
704 Brazil/SPBR-02/2020 (MOI-1) and cultured for 48 h. (A) Overtime virus progeny
705 production from PBMCs infected with SARS-CoV-2. Supernatants from cultured
706 PBMCs were collected at each time point and titrated by TCID₅₀. The small
707 symbols represent individual values (5 healthy donors) and error bars depict
708 standard deviation. (B) SARS-CoV-2 progeny titers in supernatants of infected
709 PBMCs at 24 and 48 hpi, with and without treatment with 20mM NH₄Cl. (C)
710 Effects of blocking SARS-CoV-2 cell receptor ACE2 and TMPRSS2 on virus
711 progeny production. Infected PBMCs were exposed to antibody anti-ACE2 or
712 Camostat and virus progeny was titrated in supernatants at 24 hpi. (D)
713 Immunostaining for dsRNA in PBMCs cultured on poly-lysine –coated
714 coverslips 6h after SARS-CoV-2 infection. Cells were fixed, immunostained for
715 SARS-CoV-2 (red), dsRNA (cyan) and analyzed by confocal microscopy.
716 Statistical analysis was performed using one-way or two-way ANOVA. Tukey's
717 or Holm-Sidak post-tests were applied when suitable. P values < 0.05 were
718 considered significant. Magnification: 63x. Scale bars 10 μM.

719

720 **Figure 2. SARS-CoV-2 differentially infects subsets of human PBMCs in**

721 **vitro.** (A) Representative flow cytometry plots of PBMCs infected with SARS-
722 CoV-2 (24 hpi) in the presence or absence of 20mM NH₄Cl with gating in live
723 CD14⁺, CD4⁺, CD8⁺ or CD19⁺ cells. Representative histograms of the
724 fluorescence for each condition in comparison with the proper controls. The
725 gray-shaded curve indicates secondary antibody Alexa488 signal background,
726 while the dashed curve indicates the background signal in mock-infected cells.
727 The light- and dark-colored curves indicate respectively cells infected in the
728 presence and absence of NH₄Cl. Percentages of SARS-CoV-2-infected
729 monocytes (B) and lymphocytes (C), showing the average mean fluorescent
730 intensity (MFI) in the panels on the right and the frequency (%) of SARS-CoV-2-
731 infected cells in the panels on the left. Mean ± s.d. is indicated on the bar

732 graphs. Significance was determined by one-way ANOVA with Bonferroni's
733 post-test.

734

735 **Figure 3. SARS-CoV-2 infection of PBMCs increases expression of**
736 **phosphatidylserine (PS) in T lymphocytes.** (A) Representative flow
737 cytometry plots of live CD4⁺ and CD8⁺ T cells positive for Annexin V staining in
738 PBMCs from five healthy donors 24h after infection with SARS-CoV-2 (MOI= 1).
739 (B) Percentages of live lymphocytes positive for Annexin V and expressing PS
740 in the cell surface after SARS-CoV-2 *in vitro* infection. Mean \pm s.d. is indicated
741 for all bar graphs. Significance was determined by one-way ANOVA and
742 Bonferroni's post-test.

743

744 **Figure 4: Detection of SARS-CoV-2 in PBMCs from hospitalized COVID-19**
745 **patients.** (A) Representative flow cytometry plots indicating SARS-CoV-2
746 positivity of PBMCs from COVID-19 patients in comparison with isotype control
747 and healthy donors. (B) Percentages of SARS-CoV-2-infected cells from
748 COVID-19 patients (n=22) compared with background signal from healthy
749 donors (n=12) cells. Results were compared by unpaired *t*-test (p=0.008). (C)
750 Percentages of SARS-CoV-2-infected cells considering the different
751 immunophenotypes, in COVID-19 patients (n=22). (D) Immunofluorescence of
752 PBMCs from COVID-19 patients labeling for SARS-CoV-2 (red), nuclei (blue)
753 and immunophenotypes CD4, CD19 or CD14 (green). Scale bars: 50 μ M (E)
754 Heat-map indicating SARS-CoV-2-positive cell frequencies for each
755 immunophenotype, stratified by time from symptoms onset (Patient
756 number/symptoms onset (days)). Data was plotted individually for each COVID-
757 19 patient analyzed. (F) Correlation and linear regression analysis between time
758 after symptoms onset and frequencies of SARS-CoV-2-positive cells. Both 'p'
759 and 'r' values are indicated in the graphs. The best-fit line is displayed in all the
760 graphs, while the light-color area represents the confidence interval. P values
761 <0.05 were considered significant.

762

763 **Figure 5. Peripheral blood cells naturally infected by SARS-CoV-2 from**
764 **COVID-19 patients presents double-stranded RNA, a replication**
765 **intermediate.** PBMC from (A) healthy donors or (B) COVID-19 patients were

766 isolated and put on coverslips pre-treated with poly-lysine. Cells were fixed and
767 stained for SARS-CoV-2 (red), immune phenotypes as CD4, CD19 or CD14
768 (green), dsRNA (cyan) and nuclei (blue). Immunofluorescence was examined
769 using confocal microscopy. In the bottom left corner of each channel, an inset of
770 the labelling phenotype is shown. Representative images for each
771 immunophenotype, where at least two patients were analyzed. Magnification
772 63x. Scale bar 10 μ m.

773

774 **Figure 6. SARS-CoV-2 is detected in diverse immune cell types in COVID-**
775 **19 lungs.** (A, F and I) SARS-CoV-2 staining pseudocolored in green with
776 hematoxylin counterstaining. (B, G, J) Staining for the immunophenotypes
777 CD14, CD20 and CD4, respectively, pseudocolored in red. (D): Staining for IL-
778 6, pseudocolored in magenta. (C, E, H and K) Overlaid layers from the previous
779 sequential rounds of staining, with superimposed staining indicated in yellow.
780 (c', e', h' and k') Insets from the respective previous panels. Scale bars: 50 μ m.

781

782 **Figure S1. Validation of SARS-CoV-2 detection with human convalescent**
783 **serum.** Vero cells were infected with SARS-CoV-2 (MOI=1) or mock infected
784 and incubated for 48h. (A) Phase-contrast microscopy of uninfected (left panel)
785 and SARS-CoV-2-infected Vero cell monolayer showing cytopathic effect.
786 Magnification 400 \times . (B) Immunofluorescence of Vero cells infected with SARS-
787 CoV-2 or mock-infected at 48hpi, when cells were fixed and stained for GM130
788 (red), virus (green) and nuclei (DAPI). Scale bar 10 μ m.

789

790 **Figure S2. Flow cytometry (FC) of SARS-CoV-2-infected PBMCs from**
791 **healthy with labeling for SARS-CoV-2.** PBMCs from healthy donors infected
792 in vitro (MOI=1) were analyzed by FC using mouse polyclonal anti-SARS-CoV-2
793 with and without cell permeabilization. Treatment with trypsin to remove
794 surface-bound viral particles was used as an additional control. (A)
795 Representative histograms of surface and intracellular staining for SARS-CoV-
796 2, with SARS-CoV-2-infected cells in red and trypsin-treated infected cells in
797 black. (B) Comparison of intracellular and surface staining of infected cells
798 treated or not with trypsin, and non-infected cells in percentages on the left and
799 MFI on the right.

800

801 **Figure S3. Gating strategies used for immunophenotyping of SARS-CoV-**
802 **2-infected cells.** (A) Cells were initially gated to exclude doublets and to
803 exclude dead cells, using Live/Dead APC/H7 and CD3 staining. Next, detection
804 of SARS-CoV-2 antigens in live T lymphocytes was defined based on the
805 background secondary antibody signal (Alexa488) and signal obtained in
806 healthy donors (flow plots and representative histograms). The same strategy
807 was used for CD19⁺ B lymphocytes. (B) Live monocytes were initially gated as

808 described for lymphocytes. Next, expression of CD14 and CD16 was used to
809 define circulating monocyte subpopulations. Expression of CCR2 by CD14⁺ and
810 CD14⁺CD16⁺ cells was used to define inflammatory monocytes. Among every
811 defined subpopulation, expression of SARS-CoV-2 antigens was defined in
812 comparison with secondary antibody background and healthy donors staining
813 (flow plots and representative histograms).

814

815 **Figure S4. Percentage of lymphocytes expressing phosphatidylserine (PS)**
816 **on the surface after in vitro infection with SARS-CoV-2.** Cells were analyzed
817 independently of Live/Dead APC/H7 staining. Mean \pm s.d. is shown for all bar
818 graphs. Significance was determined by one-way ANOVA and Bonferroni's
819 post-test was applied.

820

821 **Figure S5. T CD8 lymphocytes are rarely detected with SARS-CoV-2.** (A)
822 PBMC from COVID-19 patients were put on coverslips pre-treated with poly-
823 lysyne, fixed and stained for SARS-CoV-2 (red), CD8 (green) and nuclei (blue).
824 Coverslips were analyzed in epifluorescence microscopy. Magnification 400x.
825 Scale bar 20 μ m. (B) dsRNA detection in CD8 cells. PBMC was labeled as
826 described in (a) and dsRNA (cyan) using an anti-J2 antibody. At the bottom left
827 corner an inset is shown. Coverslips were analyzed in confocal microscopy.
828 Magnification 63x. Scale bar 10 μ m.

829

830 **Figure S6. Immunohistochemistry for SARS-CoV-2 antigens in *post***
831 ***mortem* lungs from COVID-19.** (A) *Post mortem* lung fragment from a
832 hantavirus fatal case obtained in 2016, as a negative control for SARS-CoV-2
833 staining. (B) Staining for SARS-CoV-2 in lung from COVID-19 fatal case. (b')
834 Individual cells showing strong cytoplasmic staining for SARS-CoV-2 antigens
835 in detail. Scale bars: 50 μ M.

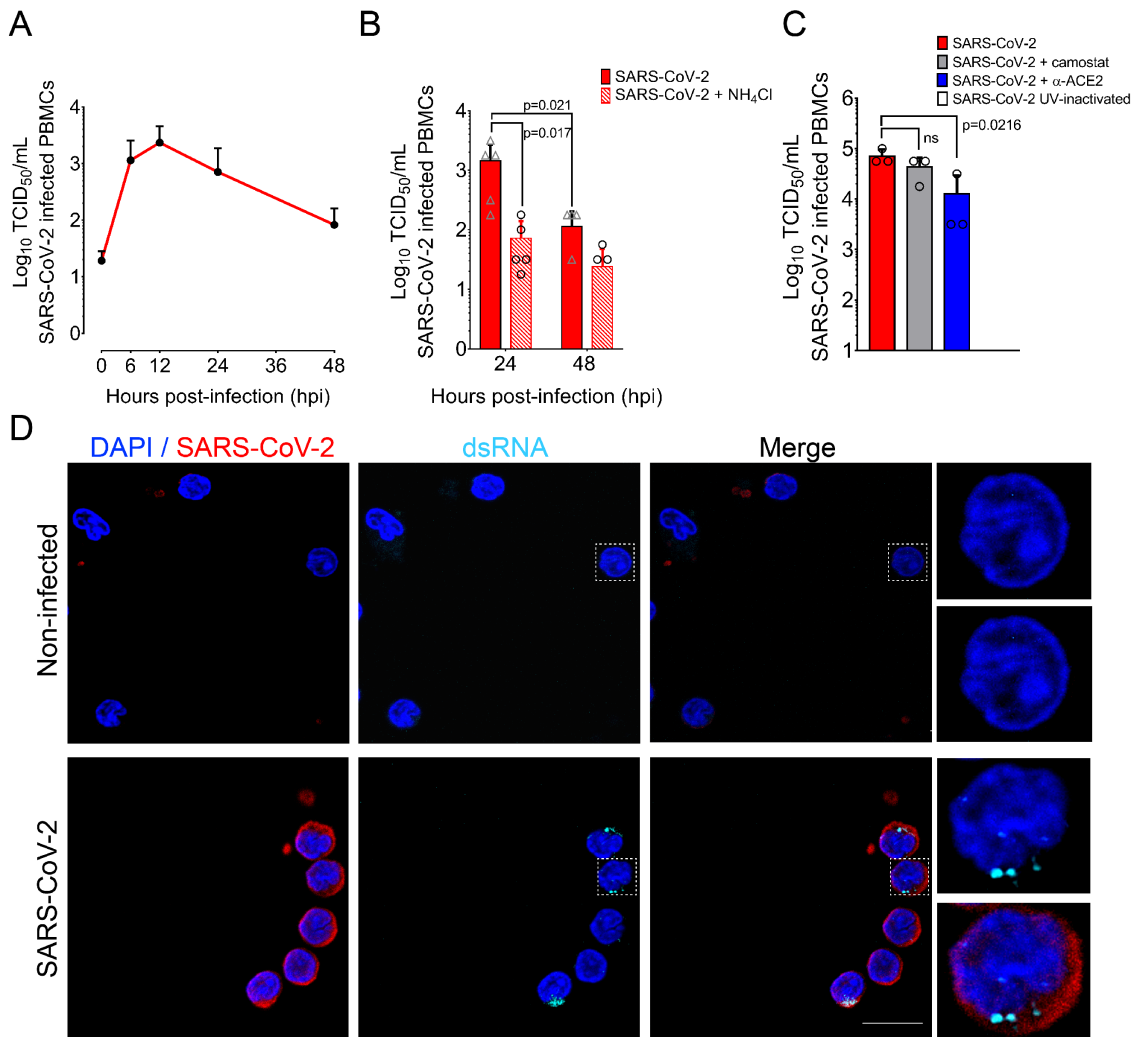
836

837

838

839 **Figure 1**

840



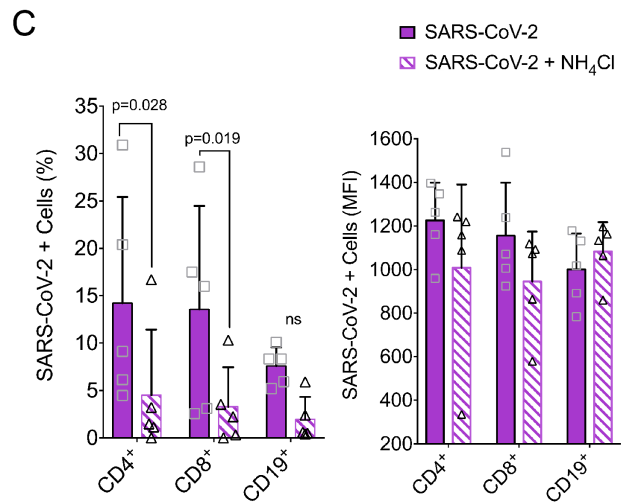
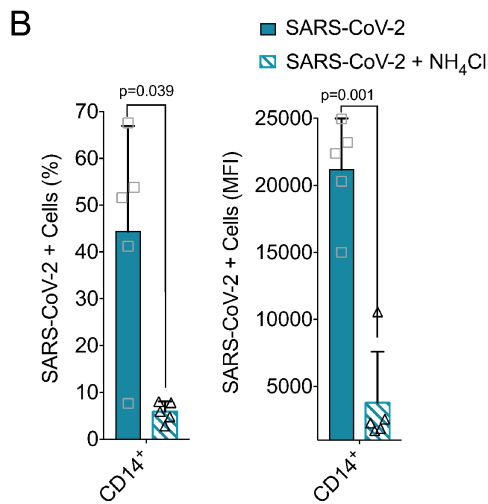
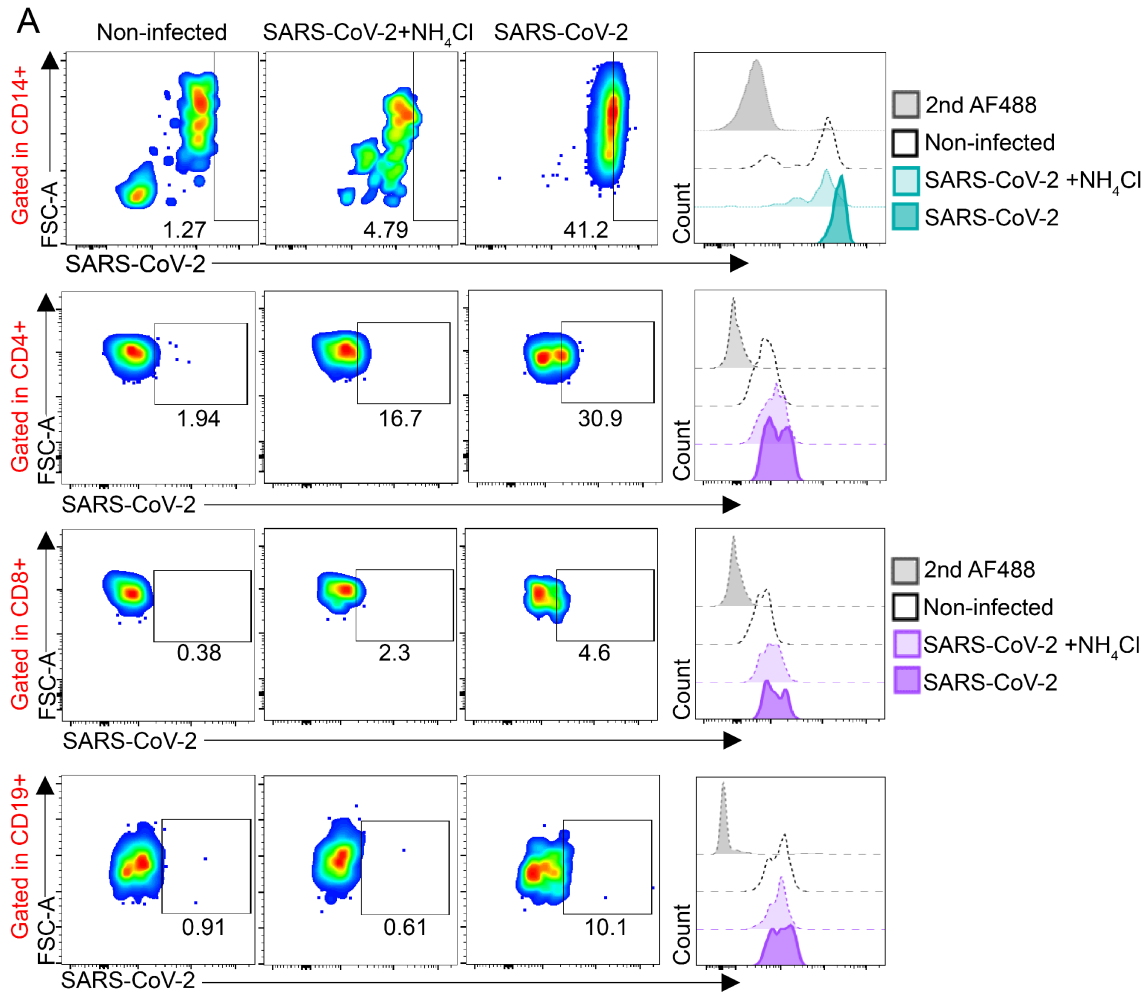
841

842

843

844

845 **Figure 2**



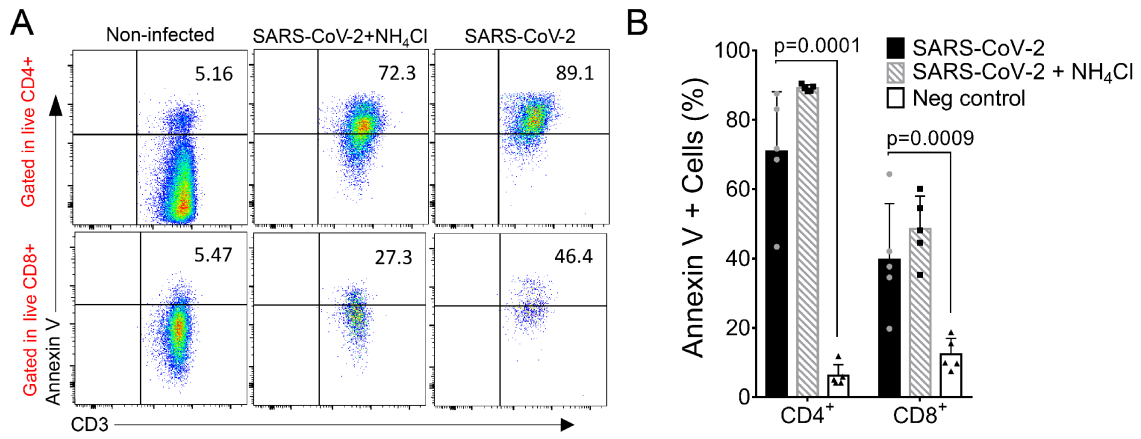
846

847

848

849 **Figure 3**

850



851

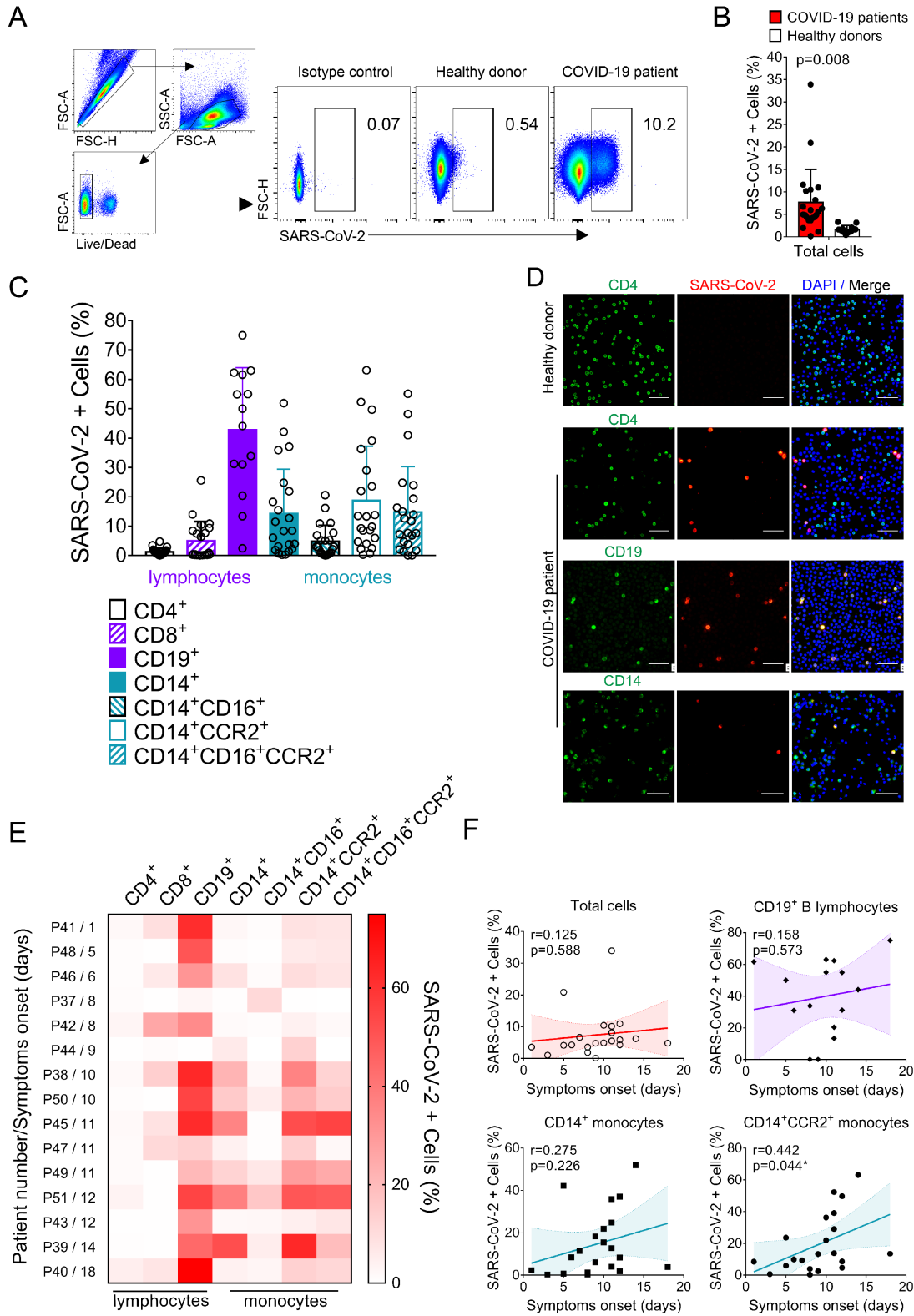
852

853

854

855 **Figure 4**

856

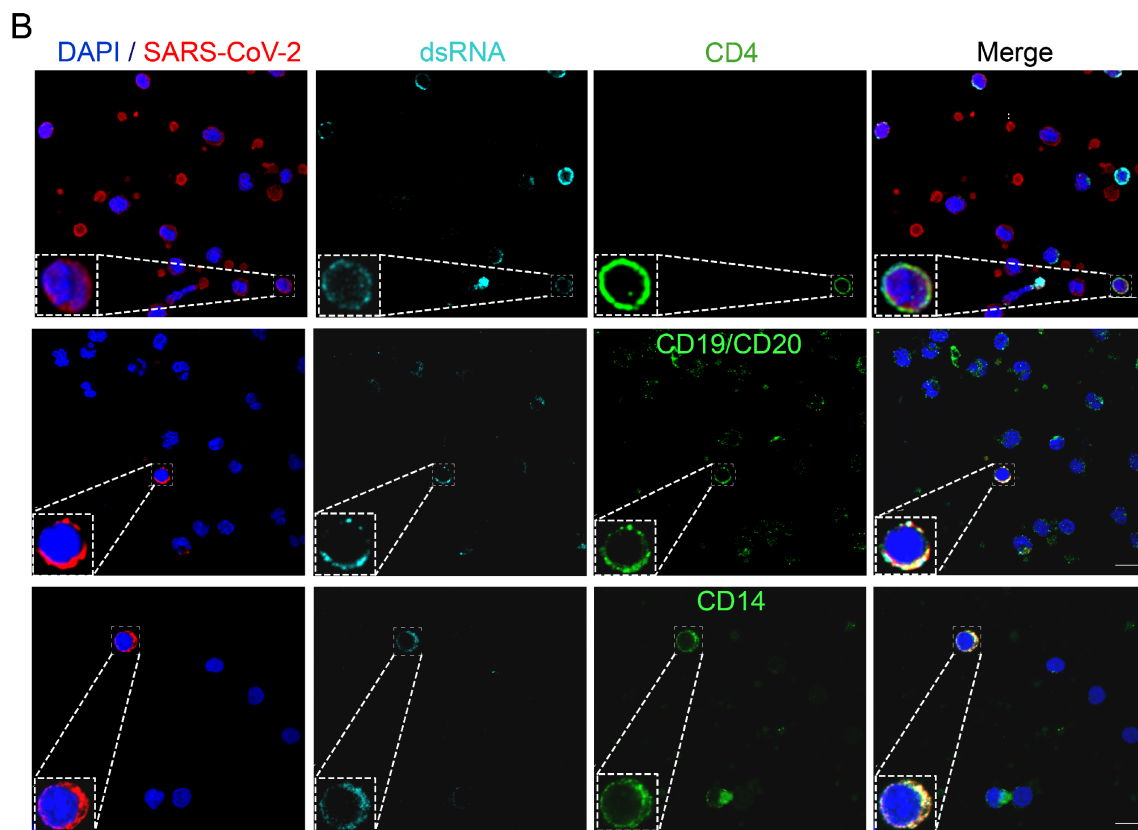
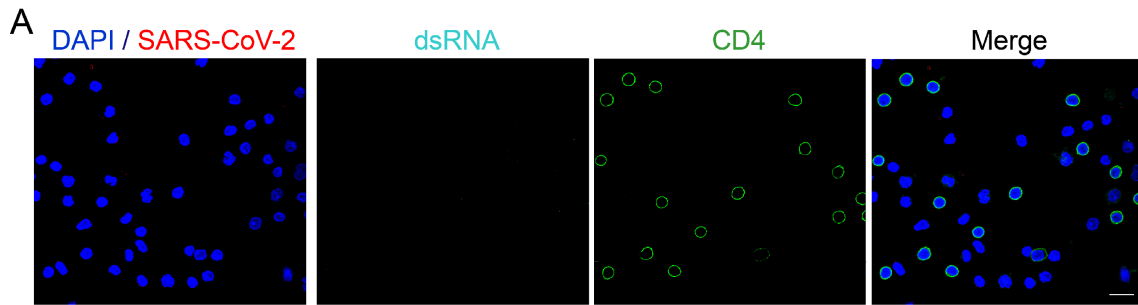


857

858

859 **Figure 5**

860

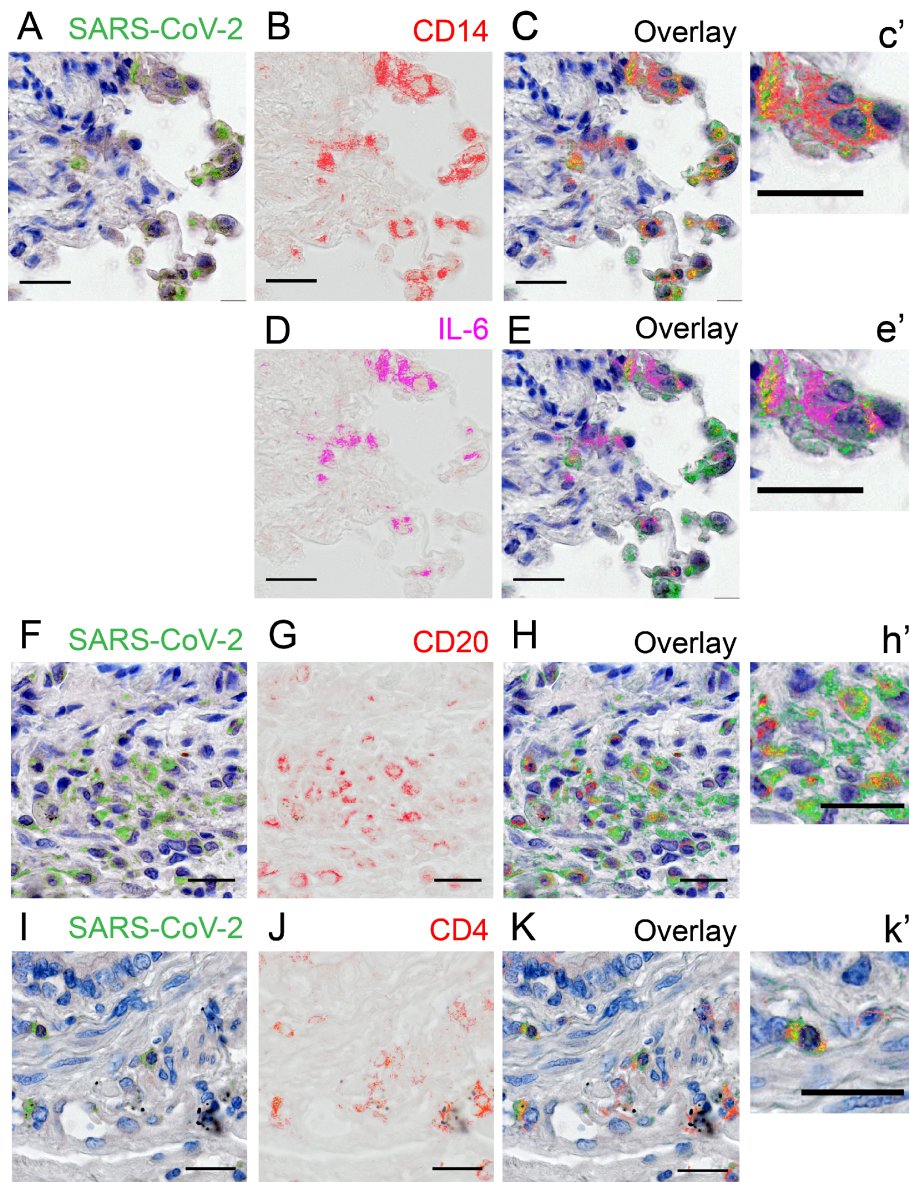


861

862

863 **Figure 6**

864



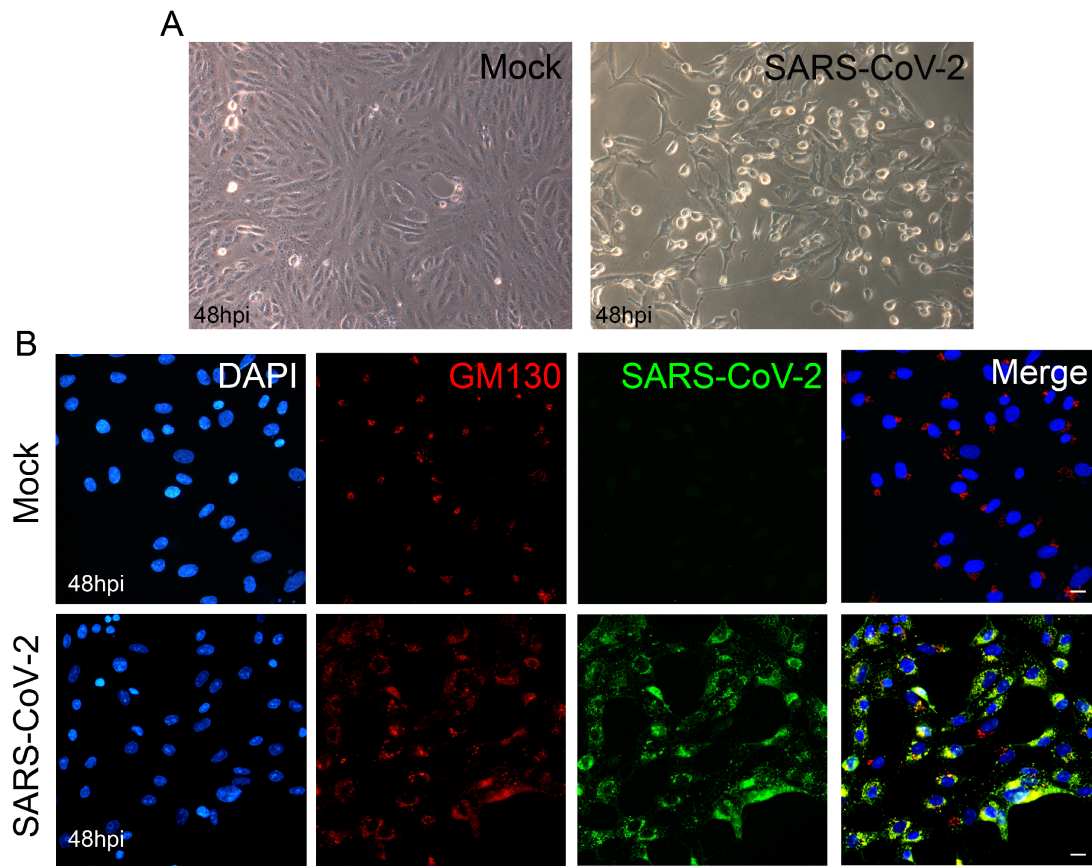
865

866

867

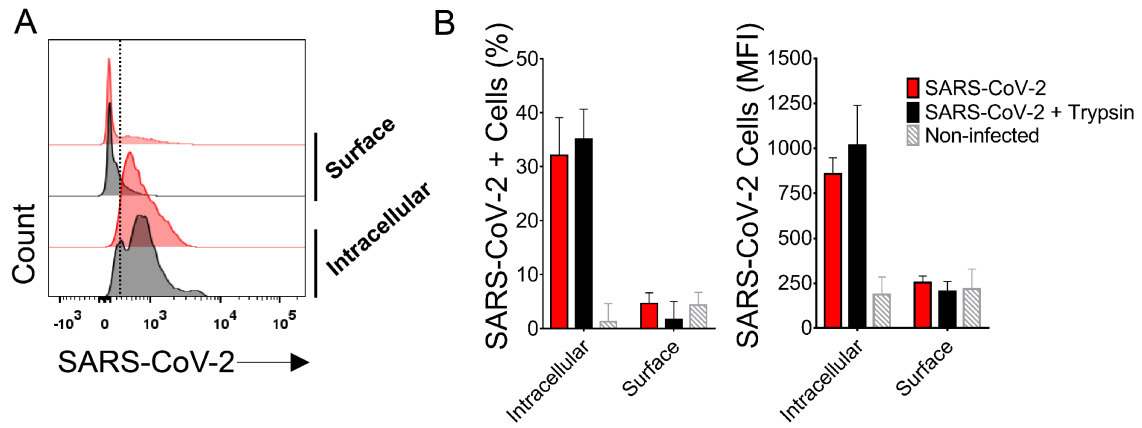
868 **Figure S1**

869



873 **Figure S2**

874

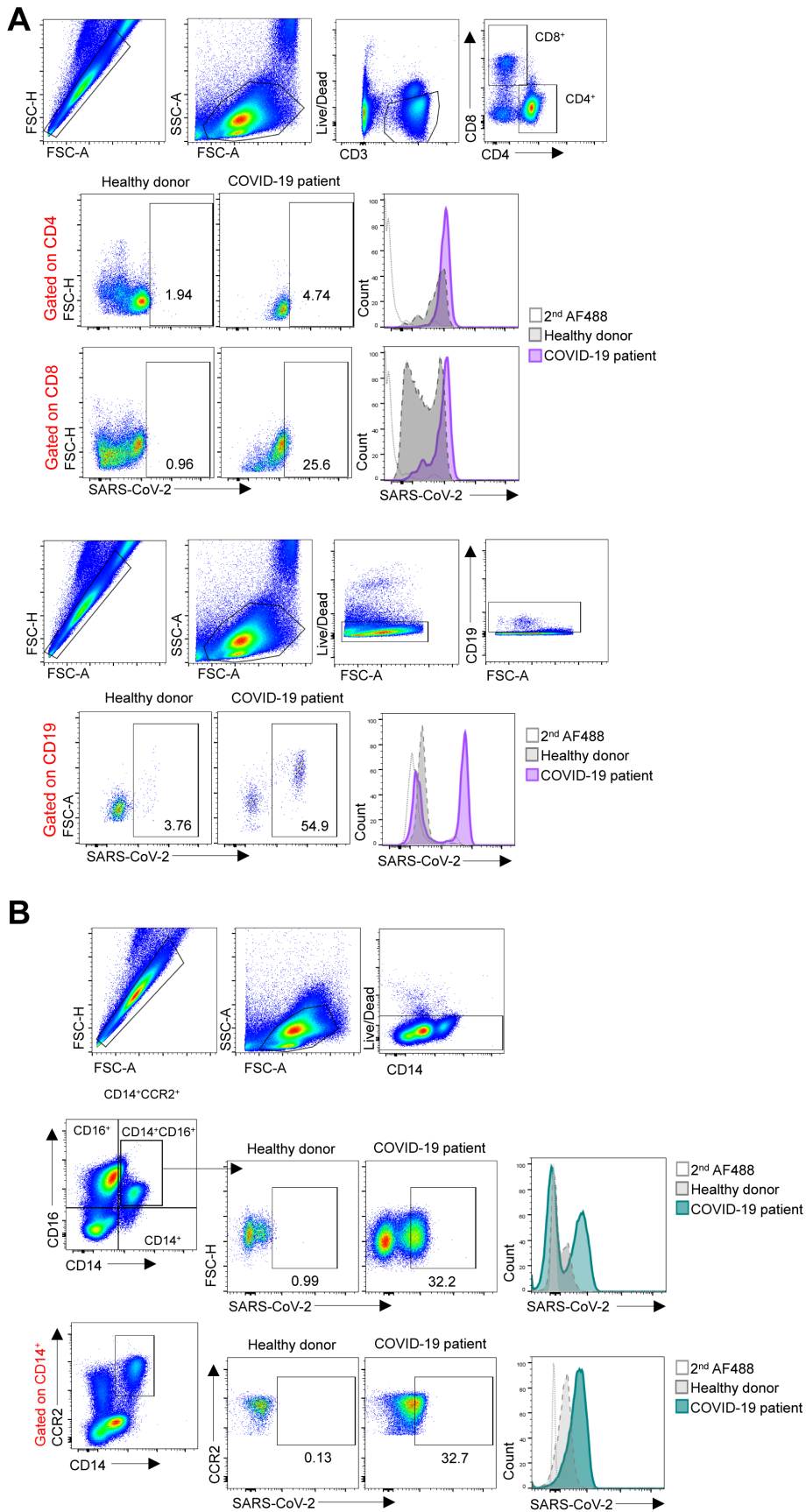


875

876

877

878 **Figure S3**

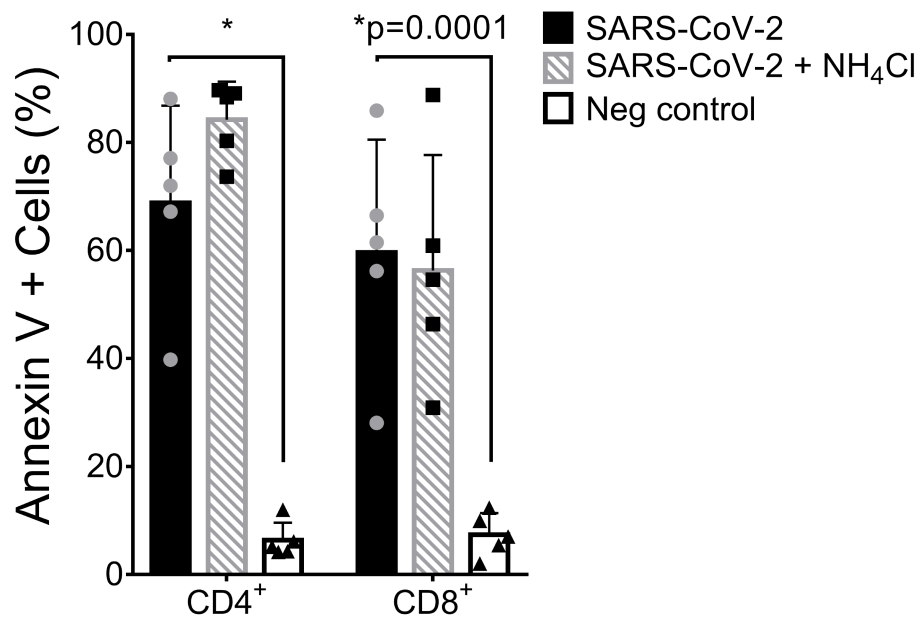


879

880

881 **Figure S4**

882



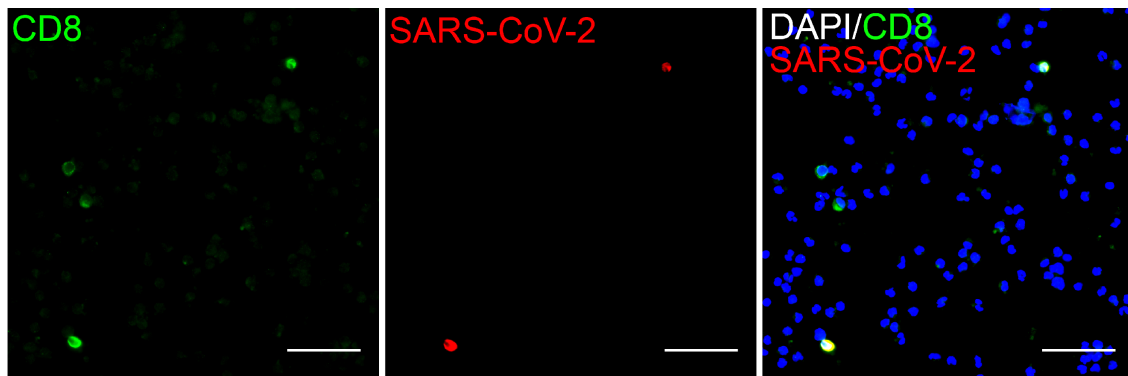
883

884

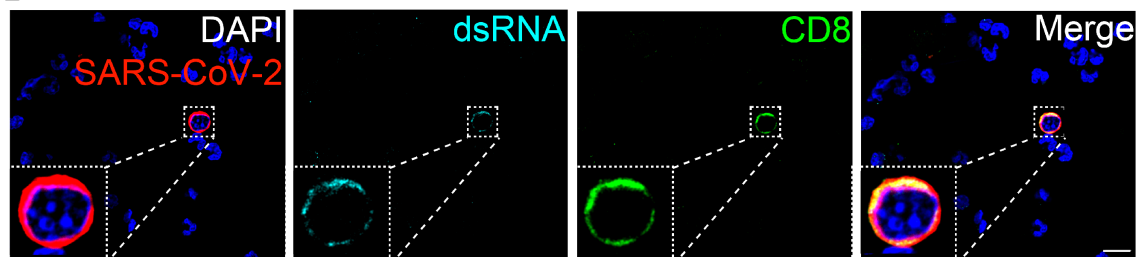
885 **Figure S5**

886

A



B

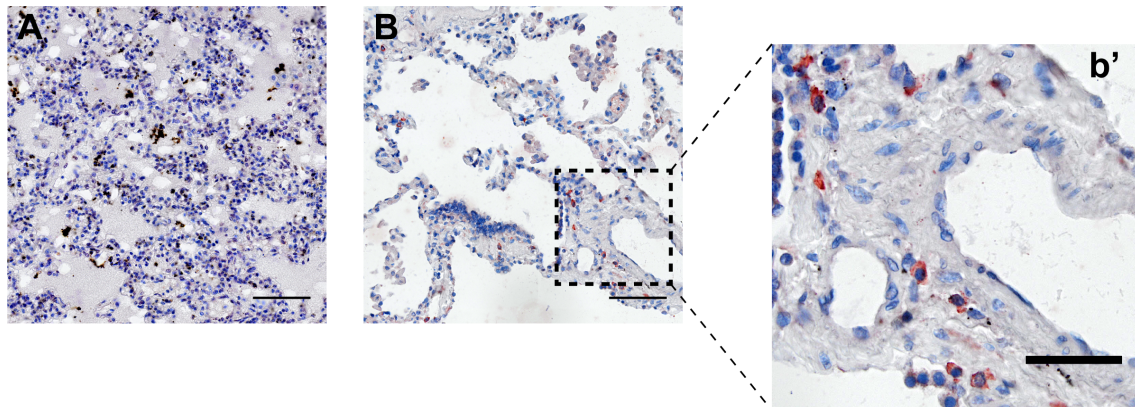


887

888

889 **Figure S6**

890



891

892

893

894 **Supplementary Tables**

895

896 **Supplementary Table 1. COVID-19 patient characteristics**

Demographics		%
Number	29	
Age (years)	61.89 \pm 17.10	
Hospital day	9.35 \pm 4.138	
Female	13	44%
Comorbidities		
Hypertension	16	55%
Diabetes	13	44%
Obesity	13	44%
Lung disease	4	14%
History of smoking	9	31%
Heart disease	7	24%
Kidney disease	2	7%
History of stroke	2	7%
Cancer	4	14%
Autoimmune diseases	2	7%
Immune deficiency	2	7%
Laboratorial findings		
CRP (mg/dL)*	14.41 \pm 8.11	
D-Dimers (μ g/mL)**	2,244 \pm 1,698	
LDH (U/L)#	749,4 \pm 490,5	
Ferritin (ng/mL)&	1,985 \pm 2836	
Haemoglobin (g/dL)	12.16 \pm 2.62	
Neutrophils (cell/mm ³)	7,521 \pm 4,952	
Lymphocytes (cell/mm ³)	1,666 \pm 1,286	
Platelets (count/mm ³)	231,009 \pm 136,433	
Image findings (n)	29	100%
Medications		
Antibiotics	29	100%
Heparin	29	100%
Antimalarial	3	10%
Oseltamivir	11	37%
Glucocorticoids	16	55%
Respiratory status		
Mechanical ventilation	24	83%
Nasal-cannula oxygen	27	93%
Room air	0	
pO ₂	70.36 \pm 45.64	
SatO ₂	82.71 \pm 18.58	
Outcome		
Deaths	9	31%

897

898

899

*CRP: C-reactive protein (Normal value <0.5 mg/dL); **D-dimers (NV <0.5 μ g/mL); #LDH: lactic dehydrogenase (Normal range: 120-246 U/L); &Ferritin (NR: 10-291 ng/mL)

900

901 **Supplementary Table 2. Viral loads of SARS-CoV-2 in PBMCs from COVID-**
902 **19 patients tested by real-time RT-PCR**

903

Patient ID	Mean viral load Genome copies/total RNA (μg)
P39	68560
P42	22770
P43	20782
P45	36507
P46	22140
P47	94736
P48	26455
P50	16396
Mean\pms.d.	38543\pm28114

904

905

906